Numerical investigation of on-chip wavelength conversion based on $InP/In_{1-x}Ga_xAs_yP_{1-y}$ semiconductor waveguide platforms

Jin Wen[1, 5, 6*], Kang Li[2], Yongkang Gong[3], Bethan Copner[2], Ben Hughes[4], Michael A. Campbell[4], Mattia Lazzaini[4], Lina Duan[1], Chengju Ma[1], Wei Fan[1], Zhenan Jia[1, 5, 6], Haiwei Fu[1, 5, 6] and Nigel Copner[2]

[1]*School of Science, Xi'an Shiyou University, Xi'an 710065, China*

[2]*Wireless and Optoelectronics Research and Innovation Centre, Faculty of Computing, Engineering and Science, University of South Wales, CF37 1DL, United Kingdom*

[3]*School of Physics and Astronomy, Cardiff University, Cardiff, CF24 3AA, United Kingdom*

[4]*National Physical Laboratory, Hampton Road, Teddington, Middlesex, TW11 0LW, United Kingdom*

[5]*Shaanxi Engineering Research Center of Oil and Gas Resource Optical Fiber Detection, Xi'an 710065, China*

[6]*Shaanxi Key Laboratory of Measurement and Control Technology for Oil and Gas wells, Xi'an 710065, China*

**Corresponding author: wenjin@xsyu.edu.cn*

Abstract

We design the high confinement $InP/In_{1-x}Ga_xAs_yP_{1-y}$ semiconductor waveguides and investigate the effective wavelength conversion based on this platform. Efficient confinement and mode field area fluctuation at different wavelength is analyzed to achieve the high nonlinear coefficient. The numerical results show that nearly zero phase-mismatch condition can be satisfied through dispersion tailoring of $InP/In_{1-x}Ga_xAs_yP_{1-y}$ waveguides, and the wavelength conversion ranging over 40 nm with the maximum conversion efficiency -26.3 dB is achieved. Meanwhile, the influences of the doping parameter y and pumping wavelength on the bandwidth and conversion efficiency are also discussed and optimized. Our demonstration of the excellent all-optical wavelength conversion properties of the $InP/In_{1-x}Ga_xAs_yP_{1-y}$ waveguides could pave the way towards direct integration telecom band devices on stand semiconductor platforms.

Key words: $InP/In_{1-x}Ga_xAs_yP_{1-y}$ waveguide; wavelength conversion; four-wave mixing; nonlinear optics

1. Introduction

Integration of III-V light emitters and amplifiers on silicon substrates is the dominated method for high-functionality and low-cost photonic integrated circuits [1, 2]. III-V nano-lasers with extremely compact footprint and ultra-low dissipation could benefit silicon-based photonic integrated circuits in terms of integration density and power consumption [3-5]. To be compatible with passive devices, the light source must emit at the transparent wavelength window to minimize the propagation loss. Meanwhile, the minimum coupling loss of fibers need light emitting at the suitable wavelength bands [6]. Some studies have been reported in extending the laser spectra and reducing the loss based on III-V semiconductor platforms [7, 8]. In particular, the room-temperature InP/InGaAs nano-ridge lasers grown on silicon substrates have been demonstrated experimentally [9]. To fully exploit the integration of devices based on InP wafer, the active material should be designed carefully to bridge the light source and other passive devices. To this end, InP wafer is promising platform candidate for monolithic integration of active and passive devices compared with silicon wafer because silicon is an indirect band gap semiconductor and thus has a very low light emission efficiency [10]. Additionally, wavelength conversion based on III-V material such as InGaAsP on InP wafer can greatly extend the wavelength range through nonlinear process such as four-wave mixing [11], which can find potential applications in various fields since the III-V source can generate stable room-temperature lasing at the telecom band [12-14]. Moreover, the InGaAsP/InP wafer allows strong on-chip mode confinement and can be directly integrated with the III-V laser source with low coupling loss compared with the devices based on silicon platforms [15-17]. Recently, research shows that the carrier lifetime in III-V semiconductor materials can be reduced to as low as 0.42 ps [18], which can reduce the nonlinear loss in the telecom band and has potential for efficient wavelength conversion.

The semiconductor material $In_{1-x}Ga_xAs_yP_{1-y}$ has generated much interest since it can be grown on InP without lattice mismatch over the composition range 0≤y≤1 provided x=0.466y [19]. Study recently shows that the band-gap energy E_g and band-gap wavelength λ_g of the $In_{1-x}Ga_xAs_yP_{1-y}$ (y=0.8, x=0.37) matched to InP can be tuned to 0.85 eV and 1459 nm respectively, which indicates that the wavelength conversion in telecom band is feasible [20]. Furthermore, nonlinear effects such as self-phase modulation, four-wave mixing and nonlinear absorption measurements at the pump wavelength 1568 nm in InP/InGaxAsP waveguides are performed experimentally, which indicate that InGaAsP has a high potential as a platform for nonlinear photonic devices [21]. Moreover, the refractive index between the InP cladding and $In_{1-x}Ga_xAs_yP_{1-y}$ core can provide relatively high refractive index contrast for better mode confinement. These features can further overcome the difficulties of on-chip integration of the III-V on SOI caused by the high nonlinear loss in telecom band and coupling loss. Therefore, the $InP/In_{1-x}Ga_xAs_yP_{1-y}$ waveguides can be used as the candidates to realize wavelength conversion with highly integrated device.

In this work, we propose and design $InP/In_{1-x}Ga_xAs_yP_{1-y}$ waveguides for the wavelength conversion under the condition of low phase-mismatch. In our design, $In_{1-x}Ga_xAs_yP_{1-y}$ quantum-well waveguides based on InP wafer can be obtained [20, 22]. Meanwhile, highly confinement of the waveguides are realized and optimized to reach effective mode area. The numerical results demonstrate efficient wavelength conversion with the efficiency up to -26.3 dB in over 40 nm wavelength range. The pump power used is 100 mW and the length of waveguide is just 5 mm, which realizes the relative lower power consumption and compact device on $InP/In_{1-x}Ga_xAs_yP_{1-y}$ platforms.

2. Design and numerical modeling

The $InP/In_{1-x}Ga_xAs_yP_{1-y}$ waveguide has the good confinement in the near telecom wavelength range. The refractive index of $In_{1-x}Ga_xAs_yP_{1-y}$ ($0 \le y \le 1$, $x=0.466y$) can be calculated as shown in Fig. 1 (a) [23]. The refractive index of the $In_{0.63}Ga_{0.37}As_{0.8}P_{0.2}$ is 3.58 at 1550 nm. Meanwhile, the refractive index of the InP is described as shown in Fig. 1 (a) and the refractive index of InP is 3.17 at 1550 nm. The refractive index increase as the value of doping parameter y enhances, which is caused by the high refractive index ratio doped GaAs on the InP wafer. The scheme of the waveguide is shown in Fig. 1 (b), the upper cladding and lower cladding is the InP and the core is the $In_{1-x}Ga_xAs_yP_{1-y}$, respectively. This kind of design can cause high confinement due to the high refractive index contrast. From the viewpoint of fabrication, this kind of InP/$In_{1-x}Ga_xAs_yP_{1-y}$ waveguide structure can be easily realized [24]. The parameters of the waveguide are as following: W is the width of the InP/$In_{1-x}Ga_xAs_yP_{1-y}$ waveguide and h is the height of the core $In_{1-x}Ga_xAs_yP_{1-y}$. While h_1 and h_2 is the height of the upper cladding and lower cladding of InP, respectively. The width and height of InP wafer substrate is 5 μm and 6 μm, respectively.

We use the COMSOL software and finite element method (FEM) [25] to calculate the TE mode distribution of the InP/$In_{0.63}Ga_{0.37}As_{0.8}P_{0.2}$ (y=0.8, x=0.37) waveguide at 1550 nm with the parameters W=2 μm, h_1=500 nm, h=250 nm and h_2=1000 nm, respectively. As shown in Fig. 1 (c), the mode distribution is focused on the core $In_{1-x}Ga_xAs_yP_{1-y}$ and nearly no mode distribution is leaked to the InP cladding. The calculated effective mode area at 1550 nm for TE mode is A_{eff}=0.73 μm^2. Meanwhile, the effective refractive index of the InP/$In_{1-x}Ga_xAs_yP_{1-y}$ waveguide n_{eff} and the effective mode area A_{eff} for TE mode variation as the wavelength is shown in Fig. 1 (d) based on the scheme of the waveguide as shown in Fig. 1 (b). When we obtain the effective mode area (for TE mode), it is aimed to realize the maximum light confinement and minimize the effective mode area A_{eff} in the waveguides given by [26].

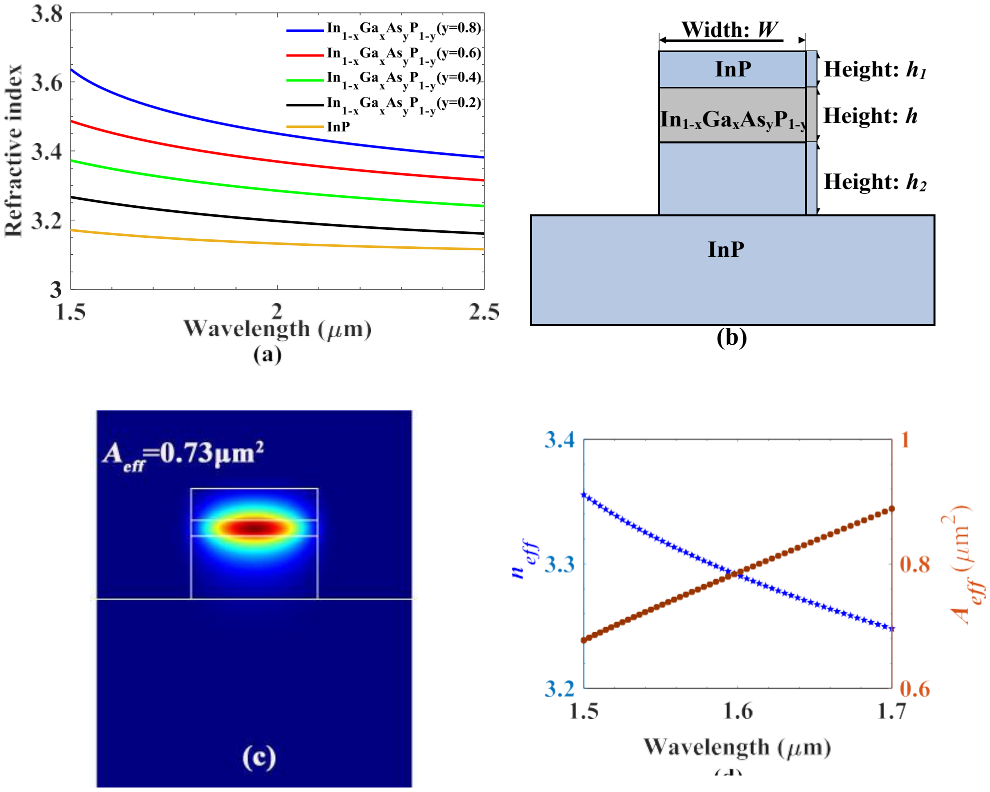

Fig. 1 (a) Theoretical values of refractive index for $In_{1-x}Ga_xAs_yP_{1-y}$ and InP as a function of wavelength and y increments of 0.2. (b) Structure of designed InP/$In_{1-x}Ga_xAs_yP_{1-y}$ waveguide. The parameters are as following: W is the width of the waveguide. Here h_1 and h_2 is the height of upper and lower InP cladding, respectively. h is the height of core $In_{1-x}Ga_xAs_yP_{1-y}$ layer. (c) Calculated TE mode distribution of the InP/$In_{1-x}Ga_xAs_yP_{1-y}$ waveguide at 1550 nm for the fixed geometry parameters as following: W=2 µm, h_1=500 nm, h=250 nm and h_2=1000 nm. A_{eff} =0.73 µm^2 is the effective mode area. (d) Calculated features of the InP/$In_{0.63}Ga_{0.37}As_{0.8}P_{0.2}$ waveguide as a function of wavelength. Red circle line: effective refractive index n_{eff} as the wavelength. Blue pentagon line: effective mode area A_{eff} as the wavelength (TE mode). The parameters of the waveguide are the same as show in Fig. 1 (c).

There are multi-parameters used to optimize for low phase-mismatch and we focus on two parameters h and h_1 to analyze the dispersion tailoring. Firstly, the parameters used in the simulation is W=2 μm, h_1=500 nm and h_2=1000 nm while the height of $In_{0.63}Ga_{0.37}As_{0.8}P_{0.2}$ changes from 200 nm to 500 nm. Based on the numerical results of effective refractive index, the propagation constant of the $InP/In_{1-x}Ga_xAs_yP_{1-y}$ waveguide can be obtained through the formula as $\beta=2\pi n_{eff}/\lambda$. Furthermore, the m^{th} dispersion parameters can be obtained through the relationship $\beta_m=d^m\beta/d\omega^m$ [26]. So we can calculate the second order dispersion coefficient β_2 and the fourth order dispersion coefficient β_4 of the $InP/In_{1-x}Ga_xAs_yP_{1-y}$ waveguide based on the numerical method. The second order dispersion coefficient β_2 and the fourth order dispersion coefficient β_4 are plotted in Fig. 2 when the parameter h changes from 200 nm to 500 nm. It is remarkably seen β_2 decreased as the h increases. However, the zero-dispersion wavelengths can't appear in the wavelength range between 1500 nm to 1700 nm, which is clearly shown in Fig. 2 (a). Meanwhile, the zero-dispersion wavelengths can be tuned to around 1550 nm under the condition of optimizing the parameters h in the range of 600 nm to 750 nm. It is found that the absolute value of β_4 is less than 0.02 ps^4/m when h changes from 200 nm to 500 nm.

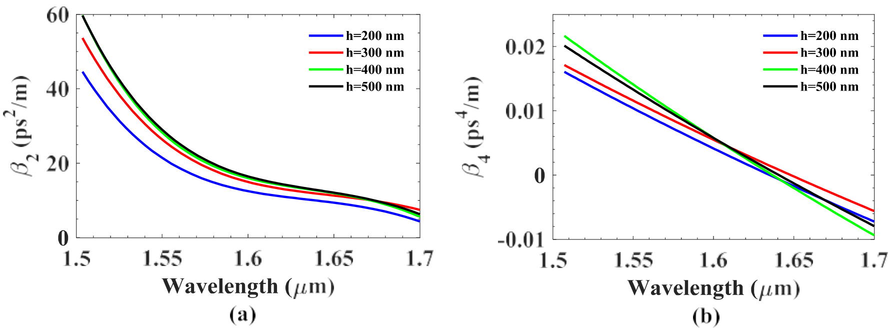

Fig. 2 High order dispersions of $InP/In_{0.63}Ga_{0.37}As_{0.8}P_{0.2}$ waveguides as function of wavelength for different value of h. (a) Second order dispersion coefficient β_2 (b) Fourth order dispersion coefficient β_4.

Additionally, the height of upper InP cladding h_1 has also the impact on the dispersion adjusting. The second order dispersion coefficient β_2 and the fourth order dispersion coefficient β_4 can be found in Fig. 3 when the height of core $In_{0.63}Ga_{0.37}As_{0.8}P_{0.2}$ is fixed at 700 nm. It is clearly shown that when the height of upper InP cladding h_1 changes from 200 nm to 500 nm, the flat dispersion curve changes to be steep around 1550 nm region as shown in Fig. 3 (a). Meanwhile, the zero-dispersion wavelength shifts to longer wavelength range. It is also found the variation of high order dispersion coefficients is small when h_1 changes from 400 nm to 500 nm, which means the optimized upper InP cladding h_1 is in this range. The numerical results indicate that impact of the h_1 on the dispersion tailoring is weak than that of h. It can be found in Fig. 3 (b) that crossover points of β_4 are different, which also demonstrates different dispersion slope for changing the parameter h and h_1.

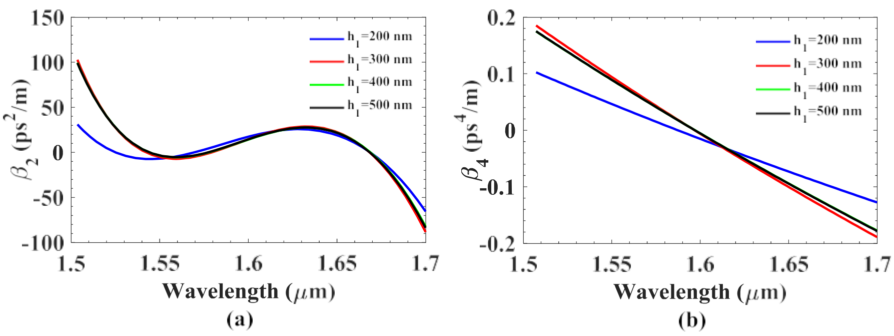

Fig. 3 High order dispersions of InP/$In_{0.63}Ga_{0.37}As_{0.8}P_{0.2}$ waveguides as function of wavelength for different value of h_1. (a) Second order dispersion coefficient β_2 (b) Fourth order dispersion coefficient β_4.

Considering the degenerate four-wave mixing condition, the modified numerical model of wavelength conversion based on InP/$In_{1-x}Ga_xAs_yP_{1-y}$ ($0\leq y\leq 1$, $x=0.466y$) waveguides platform can be given as Eqs. (1)-(3) [26, 27]:

$$\frac{dA_p}{dz} = -\frac{1}{2}\left[\alpha + \frac{\beta_{TPA}}{A_{eff}}\left(|A_p|^2 + 2|A_s|^2 + 2|A_i|^2\right)\right]A_p + i\gamma_p\left(|A_p|^2 + 2|A_s|^2 + 2|A_i|^2\right)A_p + 2i\gamma_p A_s A_i A_p^* \exp(i\Delta kz) \quad (1)$$

$$\frac{dA_s}{dz} = -\frac{1}{2}\left[\alpha + \frac{\beta_{TPA}}{A_{eff}}\left(|A_s|^2 + 2|A_p|^2 + 2|A_i|^2\right)\right]A_s + i\gamma_s\left(|A_s|^2 + 2|A_p|^2 + 2|A_i|^2\right)A_s + 2i\gamma_s A_p^2 A_i^* \exp(-i\Delta kz) \quad (2)$$

$$\frac{dA_i}{dz} = -\frac{1}{2}\left[\alpha + \frac{\beta_{TPA}}{A_{eff}}\left(|A_i|^2 + 2|A_p|^2 + 2|A_s|^2\right)\right]A_i + i\gamma_i\left(|A_i|^2 + 2|A_p|^2 + 2|A_s|^2\right)A_i + 2i\gamma_i A_p^2 A_s^* \exp(-i\Delta kz) \quad (3)$$

In Eqs. (1)-(3), A_p, A_s and A_i are the amplitude of the pump, signal and idler waves respectively and z is the propagation distance along the waveguide. We focus on the conversion efficiency and bandwidth of the wavelength conversion based on $InP/In_{1-x}Ga_xAs_yP_{1-y}$ waveguides and the pump used in the numerical simulation is continuous wave, which means the pump profile in temporal and spatial is also stable in time domain. Here α is the linear loss coefficient of the $InP/In_{1-x}Ga_xAs_yP_{1-y}$ waveguide. The second item of the left equation is the two-photon absorption and β_{TPA} is the two-photon absorption coefficient and A_{eff} is the effective mode area. The parameter $\gamma_j = 2\pi n_2/\lambda_j A_{eff}$ ($j=p, s, i$) is the nonlinear coefficient for pump, signal and idler wavelengths. Considering the effects including the self-phase modulation and cross-phase modulation, the phase mismatch Δk is given under the degenerate pump condition by [28],

$$\Delta k = 2\gamma_p P - \Delta k_{linear} \quad (4)$$

where $\gamma_p = 2\pi n_2/\lambda A_{eff}$, n_2 is the nonlinear refractive index of the waveguide. P is the pump power, $\Delta k_{linear} = 2k_p - k_s - k_i$ is the linear phase-mismatch, and k_p, k_s and k_i are the pump, signal and idler propagation constants. Considering the dispersion effects up to fourth order, the linear phase-mismatch is given by,

$$\Delta k_{linear} = -\beta_2 \Omega^2 - \frac{1}{12}\beta_4 \Omega^4 \quad (5)$$

where β_2 and β_4 are the second order dispersion coefficient and the fourth order dispersion coefficient as the description in the part of dispersion tailoring, and Ω is the frequency difference between the pump and signal waves. Through solving the nonlinear coupled equations, the conversion efficiency and bandwidth can be obtained. Here we focus the flatness and efficiency of the wavelength conversion and the conversion efficiency CE can be defined as,

$$CE = \frac{P_i^{out}}{P_s^{in}} \quad (6)$$

where P_i^{out} is the output idler power and P_s^{in} is the input signal power, respectively.

3. Results and discussion

The numerical results of wavelength conversion based on $InP/In_{1-x}Ga_xAs_yP_{1-y}$ waveguides can be obtained through solving the Eqs. (1)-(3) under the condition of dispersion tailoring, which can be solved by fourth-order Runge-Kutta method. It is pointed that pump power is 100 mW and the length of waveguide is 5 mm. The linear loss coefficient α=0.5 dB/cm, the two-photon absorption coefficient $\beta_{TPA}=1\times10^{-12}$ m/W, which dominates the nonlinear loss. The nonlinear refractive index of $InP/In_{1-x}Ga_xAs_yP_{1-y}$ waveguide given in this simulation is $n_2=2.2\times10^{-17}$ m^2/W [29]. To realize the broadband conversion efficiency, the phase-mismatch is the dominated role in the process of four-wave mixing.

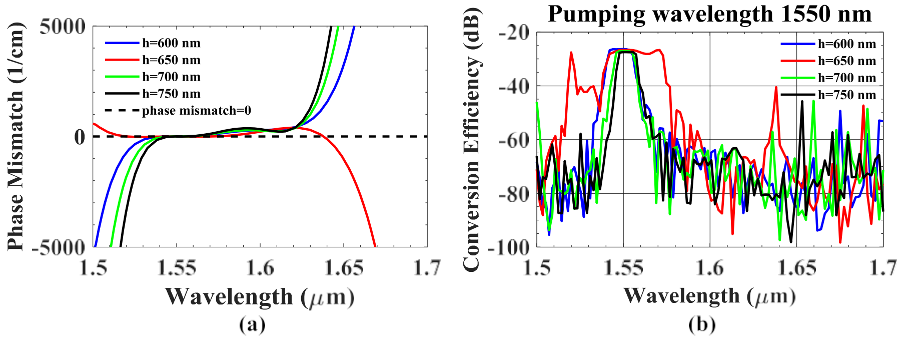

Fig. 4 (a) Phase-mismatch of the InP/$In_{0.63}Ga_{0.37}As_{0.8}P_{0.2}$ waveguides when *h* changes from 600 nm to 750 nm. (b) Conversion efficiency of InP/$In_{0.63}Ga_{0.37}As_{0.8}P_{0.2}$ waveguides. Pumping wavelength is 1550 nm. The height of $In_{0.63}Ga_{0.37}As_{0.8}P_{0.2}$ *h* changes from 600 nm to 750 nm.

The phase-mismatch can be shown as Fig. 4 (a) for different parameters of *h*. When the height of core $In_{0.63}Ga_{0.37}As_{0.8}P_{0.2}$ changes from 600 nm to 750 nm with the height of upper and lower InP cladding fixed at 500 nm and 1000 nm, respectively, the phase-mismatch condition varies markedly as shown in Fig. 4 (a). The quasi-phase matching condition can be satisfied in the broadband wavelength range. Meanwhile, the near zero phase-mismatch can be obtained from about 1.5 µm to 1.6 µm wavelength range, which means wavelength conversion can be realized under this condition. The numerical results of wavelength conversion are obtained as shown in Fig. 4 (b). In this simulation, the pump power is 100 mW, the input signal and idle power are 10 mW and 0, respectively. The pumping wavelength is fixed at 1550 nm and the length of waveguide is 5 mm. As seen in Fig. 4 (b), the conversion efficiency can reach to over -30 dB when the pump power is 100 mW. The numerical results agree with the value of phase-mismatch depicted in Fig. 4 (a). Relative flat wavelength conversion is shown when the parameter *h* is optimized in the range of 600 nm to 750 nm. The conversion bandwidth is over 40 nm with the conversion efficiency over -30 dB when h is 650 nm. Moreover, the conversion efficiency will decrease when h further increases over 700 nm, especially in the longer wavelength region.

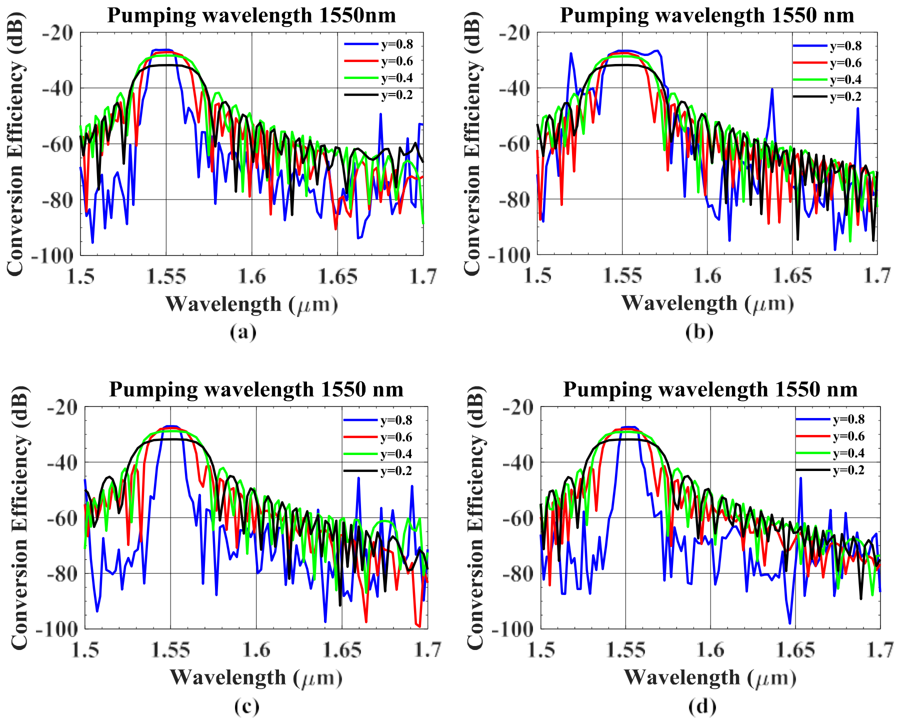

Fig. 5 Conversion efficiency of InP/$In_{1-x}Ga_xAs_yP_{1-y}$ waveguides with different doping parameters y and h. (a) The height of $In_{1-x}Ga_xAs_yP_{1-y}$ h is 600 nm. (b) The height of $In_{1-x}Ga_xAs_yP_{1-y}$ h is 650 nm. (c) The height of $In_{1-x}Ga_xAs_yP_{1-y}$ h is 700 nm. (d) The height of $In_{1-x}Ga_xAs_yP_{1-y}$ h is 750 nm. The value of doping parameter y changes from 0.2 to 0.8.

We further explore the conversion efficiency based on $In_{1-x}Ga_xAs_yP_{1-y}$ waveguides through tailoring the doping parameters y and x (x=0.466y). It can be found that when the height of $In_{1-x}Ga_xAs_yP_{1-y}$ changes from 600 nm to 750 nm, the conversion efficiency decreases as the nonlinear coefficient reduced caused by the effective mode area enhances as shown in Fig. 5 (a) to Fig. 5 (d). For the fixed parameter h, the bandwidth of wavelength conversion increases, which can be obviously compared for y=0.8 and y=0.2 in Fig. 5. The maximum of conversion efficiency is -26.3 dB under the condition of pump power 100 mW. When the value of doping parameters y changes from 0.8 to 0.2, the refractive index of $In_{1-x}Ga_xAs_yP_{1-y}$ reduces as the same trend of the effective index of $InP/In_{1-x}Ga_xAs_yP_{1-y}$ waveguide. The light confinement will reduce as the value of y decrease to nearly the same as the upper and lower cladding InP (as shown in Fig. 1 (a)), which gives rise to the enhance value of A_{eff}. The conversion efficiency reduces as the value of doping parameter y decreases. On the other hand, the reduced effective refractive index of $InP/In_{1-x}Ga_xAs_yP_{1-y}$ waveguide causes the lower effective refractive index contrast Δn_{eff} between the 1.5 μm and 1.7 μm wavelength range, which changes the dispersion and phase matching condition.

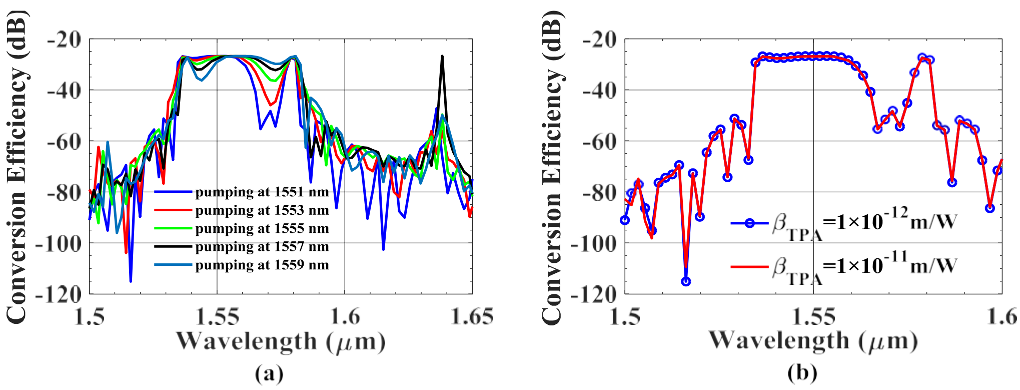

Fig. 6 (a) Wavelength conversion based on the $InP/In_{1-x}Ga_xAs_yP_{1-y}$ (y=0.8, x=0.466y) waveguides as the function of pumping wavelength. The pumping wavelength changes from 1551 nm to 1559 nm. (b) Wavelength conversion based on the $InP/In_{1-x}Ga_xAs_yP_{1-y}$ (y=0.8, x=0.466y) waveguides as the function of two-photon absorption β_{TPA} when the the pumping wavelength is fixed at 1551 nm. The parameters of the $InP/In_{1-x}Ga_xAs_yP_{1-y}$ waveguide are as following: W=2 μm, h_1=500 nm, h=670 nm and h_2=1000 nm.

To explore the influence of the pumping wavelength on the conversion efficiency and bandwidth, we change the pumping wavelength from 1551 nm to 1559 nm with increment 2 nm. In this simulation, the parameters of InP/$In_{1-x}Ga_xAs_yP_{1-y}$ (y=0.8, x=0.466y) waveguide are fixed as following: the width of waveguide W=2 μm, the height of upper InP h_1=500 nm, the height of lower InP h_2=1000 nm and the height of $In_{1-x}Ga_xAs_yP_{1-y}$ is h=670 nm. It can be found that the maximum conversion efficiency is about -26.9 dB as shown in Fig. 6 (a), which keeps the same value whatever the pumping wavelength changes. Meanwhile, a peak conversion efficiency can be found at about 1640 nm caused by the quasi-phase matching condition. When the pumping wavelength is fixed at 1551 nm, the bandwidth of wavelength conversion is about 20 nm. The bandwidth increases as the pumping wavelength changes to longer wavelength region with increment 2 nm. It can be observed when the pumping wavelength is 1559 nm, the bandwidth extends to 40 nm. It is clearly shown the bandwidth of wavelength conversion enhances when the pumping wavelength extends to longer wavelength range with more flatness significantly. This phenomenon can be explained the near zero phase-matching condition can be satisfied in broadband wavelength range through adjusting the pumping wavelength just 8 nm. Fig. 6 (b) depicts the effect of the two-photon absorption β_{TPA} on the conversion efficiency of InP/$In_{1-x}Ga_xAs_yP_{1-y}$ waveguides when the pumping wavelength is fixed at 1551 nm. It can be found that the conversion efficiency decreases to some extent when the value of β_{TPA} changes from 1×10^{-12} m/W to 1×10^{-11} m/W. The numerical results show that the bandwidth is not affected by the changing of β_{TPA}.

4. Conclusions

We numerically investigate InP/$In_{1-x}Ga_xAs_yP_{1-y}$ waveguide to realize wavelength conversion ranging over 40 nm with the maximum conversion efficiency -26.3 dB. Dispersion tailoring of the InP/$In_{1-x}Ga_xAs_yP_{1-y}$ waveguides is discussed to reveal the impacts on the wavelength conversion. The numerical results show that the phase-mismatch can be reduced through dispersion tailoring in broadband wavelength range under the condition of fixed pump power. As the value of doping parameter y decrease, the bandwidth of wavelength conversion increases remarkably due to the flexible refractive index distribution in the process of changing doping parameter y. Meanwhile, it is found that the relative flat wavelength conversion can be obtained through adjusting pumping wavelength in 8 nm (from 1551 nm to 1559 nm). This research can be applied in design and optimization of nonlinear optics.

Acknowledgments

This work was supported by the National Natural Science Foundation of China under Grant No. 61505160, the Innovation Capability Support Program of Shaanxi (Program No. 2018KJXX-042), the Natural Science Basic Research Program of Shaanxi (Program No. 2019JM-084), the 2015 Foshan Technology Innovation Group Project (Advanced Solid State Light Source Application and Innovation Team) and the National Physical Laboratory Directors' Science and Engineering Fund Investigators Award (project number 06. 2019).

References

[1]. Z. Zhou, B. Yin, and J. Michel, “On-chip light sources for silicon photonics,” Light Sci. Appl. 4, e358 (2015).

[2]. D. Liang and J. Bowers, “Recent progress in lasers on silicon,” Nat. Photon. **4**, 511-517 (2010).

[3]. R. Chen, T. Tran, K. Ng, W. Ko, L. Chuang, F. Sedgwick, and C. Chang-Hasnain, “Nanolasers grown on silicon,” Nat. Photon. **5**, 170-175 (2011).

[4]. B. Mayer, L. Janker, B. Loitsch, J. Treu, T. Kostenbader, S. Lichtmannecker, T. Reichert, S. Morkotter, M. Kaniber, G. Abstreiter, and C. Gies, “Monolithically integrated high-β nanowire lasers on silicon,” Nano Lett. **16**(1), 152-156 (2015).

[5]. J. Tatebayashi, S. Kako, J. Ho, Y. Ota, S. Iwamoto, and Y. Arakawa, “Room-temperature lasing in a single nanowire with quantum dots,” Nat. Photon. **9**, 501-505 (2015).

[6]. D. Thomson, A. Zilkie, J. Bowers, T. Komljenovic, G. Reed, L. Vivien, D. Marris-Morini, E. Cassan, L. Virot, J. Fédéli, J. Hartmann, J. Schmid, D. Xu, F. Boeuf, P. O’Brien, G. Mashanovich, and M. Nedeljkovic, “Roadmap on silicon photonics,” J. Opt. **18**(7), 073003 (2016).

[7]. M. Takiguchi, A. Yokoo, K. Nozaki, M. Birowosuto, K. Tateno, G. Zhang, E. Kuramochi, A. Shinya, and M. Notomi, “Continuous-wave operation and 10-Gb/s direct modulation of InAsP/InP sub-wavelength nanowire laser on silicon photonic crystal,” APL Photon. **2**(4), 046106 (2017).

[8]. H. Kim, W. Lee, A. Farrell, A. Balgarkashi, and D. Huffaker, "Telecom-wavelength bottom-up nanobeam lasers on silicon-on-insulator," Nano Lett. **17**(9), 5244-5250 (2017).

[9]. Y. Han, W. Ng, C. Ma, Q. Li, S. Zhu, C. Chan, K. Ng, S. Lennon, R. Taylor, K. Wong, and K. Lau, "Room-temperature InP/InGaAs nano-ridge lasers grown on Si and emitting at telecom bands," Optica **5**(8), 918-923 (2018).

[10]. H. Rong, R. Jones, A. Liu , O. Cohen, D. Hak, A. Fang, and M. Paniccia, "A continuous-wave Raman silicon laser," Nature **433**, 725-728 (2005).

[11]. P. Apiratikul, J. Wathen, G. Porkolab, B. Wang, L. He, T. Murphy, and C. Richardson, "Enhanced continuous-wave four-wave mixing efficiency in nonlinear AlGaAs waveguides," Opt. Express **22**(22), 26814-26824 (2014).

[12]. S. Li, X. Zhou, M. Li, X. Kong, J. Mi, M. Wang, W. Wang, and J. Pan, "Ridge InGaAs/InP multi-quantum-well selective growth in nanoscale trenches on Si (001) substrate," Appl. Phys. Lett. **108**(2), 021902 (2016).

[13]. Y. Han, Q. Li, S. Chang, W. Hsu, and K. Lau, "Growing InGaAs quasi-quantum wires inside semi-rhombic shaped planar InP nanowires on exact (001) silicon," Appl. Phys. Lett. **108**(24), 242105 (2016).

[14]. Y. Han, Q. Li, S. Zhu, K. Ng, and K. Lau, "Continuous-wave lasing from InP/InGaAs nanoridges at telecommunication wavelengths," Appl. Phys. Lett. **111**(21), 212101 (2017).

[15]. X. Liu, R. O Jr, Y. Vlasov, W. Green, “Mid-infrared optical parametric amplifier using silicon nanophotonic waveguides,” Nat. Photon. **4**, 557-560 (2010).

[16]. E. Tien, Y. Huang, S. Gao, Q. Song, F. Qian, S. Kalyoncu, and O Boyraz, “Discrete parametric band conversion in silicon for mid-infrared applications,” Opt. Express **18**(21), 21981-21989 (2010).

[17]. J. Wen, H. Liu, N. Huang, Q. Sun, and W. Zhao, “Widely tunable femtosecond optical parametric oscillator based on silicon-on-insulator waveguides,” Opt. Express **20**(4), 3490-3498 (2012).

[18]. D. Cui, S. M. Hubbard, D. Pavlidis, A. Eisenbach, and C. Chelli, “Impact of doping and MOCVD conditions on minority carrier lifetime of zinc-and carbon-doped InGaAs and its applications to zinc-and carbon-doped InP/InGaAs heterostructure bipolar transistors,” Semicond. Sci. Technol. **17**(6), 503-509 (2002).

[19]. B. Jensen and A. Torabi, “Refractive index of quaternary $In_{1-x}Ga_xAs_yP_{1-y}$ lattice matched to InP,” J. Appl. Phys. **54**(6), 3623-3625 (1983).

[20]. S. Saeidi, K. M. Awan, L. Sirbu, and K. Dolgaleva, “Nonlinear photonics on-a-chip in III-V semiconductors: quest for promising material candidates,” Applied Optics **56**(19), 5532-5541 (2017).

[21]. S. Saeidia, P. Rasekha, K. M. Awana, A. Tüğenb, M. J. Huttunenc, K. Dolgalevaa, “Demonstration of optical nonlinearity in InGaAsP/InP passive waveguides,” Optical Materials **84**, 524-530 (2018).

[22]. J. Donnelly, H. Le, E. Swanson, S. Groves, A. Darwish, E. Ippen, "Nondegenerate four-wave mixing wavelength conversion in low-loss passive InGaAsP-InP quantum-well waveguides," Photonics Technology Letters **8**(5), 623-625 (1996).

[23]. B. Jensen, A. Torabi, "Quantum theory of the dispersion of the refractive index near the fundamental absorption edge in compound semiconductors," IEEE J. Quantum Elect. **19**(3), 448-457 (1983).

[24]. Y. Han, Q. Li, and K. M. Lau, "Highly ordered horizontal indium gallium arsenide/indium phosphide multi-quantum-well in wire structure on (001) silicon substrates," J. Appl. Phys. **120**(24), 245701 (2016).

[25]. J. Jin, *The Finite Element Method in Electromagnetics* (John Wiley and Sons, New York, 1993).

[26]. G. P. Agrawal, *Nonlinear Fiber Optics*, 3rd ed. (Academic, San Diego, 2001).

[27]. W. Mathlouthi, H. Rong, M. Paniccia, "Characterization of efficient wavelength conversion by four-wave mixing in sub-micron silicon waveguides," Optics Express **16**(21), 16735-16745 (2008).

[28]. M. Foster, A. Turner, R. Salem, M. Lipson, and A. Gaeta, "Broad-band continuous-wave parametric wavelength conversion in silicon nanowaveguides," Opt. Express **15**(20), 12949-12958 (2007).

[29]. P. Yupapin, B. Vanishkorn, "Mathematical simulation of light pulse propagating within a microring resonator system and applications," Applied Mathematical Modelling **35**(4), 1729-1738 (2011).